Automated Tactical Maneuver Discovery, Reasoning and Trajectory Planning for Autonomous Driving

Tianyu Gu[†], John M. Dolan[†,‡] and Jin-Woo Lee[†]

***Abstract*— In a hierarchical motion planning system for urban autonomous driving, it is a common practice to separate tactical reasoning from the lower-level trajectory planning. This separation makes it difficult to achieve robust maneuver-based tactical reasoning, which is intrinsically linked to trajectory planning. We therefore propose a planning method that automatically discovers tactical maneuver patterns, and fuses pattern reasoning and sampling-based trajectory planning. The results demonstrate enhanced planning feasibility, coherency and scalability.**

I. Introduction

In order to realize fully autonomous driving in urban environments[1], an autonomous vehicle is typically equipped with a hierarchical planning system to handle different aspects. As reviewed in Buehler [1], many entries in the 2007 DARPA Urban Challenge (UC) used a hierarchical planning system, in which tactical planning (a.k.a. behavior planning) and trajectory planning are separately implemented (the **separation**). The former is responsible for generating tactical decisions, while the latter generates the executable trajectory. The tactical planning can be further classified as:

- **Rule-based tactics**: speed limits, work zone, stopping at stop sign and intersection precedence handling.
- **Route-based tactics**: choose which lane to switch to in order to meet global routing requirements.
- **Maneuver-based tactic**: decide when and how to yield, follow or overtake other agents.

Rule-based and route-based tactical planning can be handled decoupled from trajectory planning with State Machines [2], [3], [4], or other Action Selection Mechanisms [5], [6]. However, the **separation** poses hard-to-reconcile challenges to implementing maneuver-based tactics with a trajectory planner:

Challenge 1: Maneuver feasibility conflict. Maneuver-based tactical planning does not explicitly guarantee plan feasibility, which may result in infeasible maneuver decisions from the perspective of the trajectory planner[2].

Challenge 2: Ignorance of the environment's topology. The neglect of the environment's topological structure by both tactical and trajectory planning can lead to inconsistent outcomes from cycle to cycle.

Challenge 3: Unscalable manual scenario discovery. It is not practical to pre-design maneuver-based tactical rules for all unforeseen situations, which can quickly become very complex with multiple objects.

This paper addresses these three challenges. To guarantee trajectory feasibility (**Challenge 1**), we divide the maneuver-based aspect from the tactical planning, and fuse it with motion planning in order to simultaneously perform tactical reasoning and trajectory planning. To incorporate topology awareness (**Challenge 2**) and remove manual tactical rule design (**Challenge 3**), we develop maneuver pattern identification that explicitly discovers and reasons about patterns.

II. Related Work

State machines or decision trees with hand-crafted rules are often used to perform maneuver-based tactical reasoning. Fig.1 illustrates two common maneuver triggering rules designed for lane-change and stop-and-go at intersections. While these rules are able to handle basic traffic situations, they are often challenged in the real world when the on-road or intersection traffic is dense. Intended maneuvers may fail due to the rules being conservatively designed in order to compensate for the fact that they do not guarantee trajectory feasibility/admissibility. Another limitation is that such predefined rules are not general and robust enough to handle varied situations, e.g., when the real-world objects do not match any pre-defined configuration template.

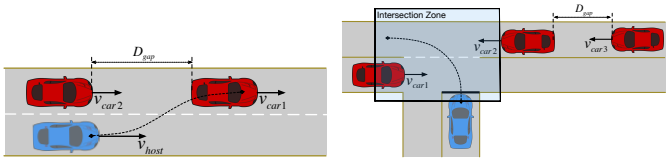

(a) Lane change **(b)** To-go at intersection

Fig. 1: Maneuver-based tactical rules for lane-change and lane-merge behaviors. In (a), lane change is triggered according to a triggering condition, e.g., D_{gap} above a certain threshold. In (b), stopping at the intersection is part of rule-based tactical planning, but going is often triggered with an empirical safety rule, like the estimated time of zone arrival T of all relevant moving targets being above a threshold.

The lower-level trajectory planners designed for UC and nearly all subsequent efforts [7], [8], [9], [10], [11], [12] aimed at optimizing (minimizing) an objective (cost) func-

[†] Electrical & Computer Engineering Department, Carnegie Mellon University, Pittsburgh, PA, USA tianyu@cmu.edu

[‡] Robotics Institute, School of Computer Science, Carnegie Mellon University, Pittsburgh, PA, USA jmd@cs.cmu.edu

[†] Research & Development, General Motors, Warren, Detroit, USA

[1]The most common driving situations considered in this paper is are on-road and at-intersection.

[2]A practical solution to reduce such inconsistency is to design conservative decision rules, but this does not provide any formal guarantee, and also comes at the price of limiting the vehicle maneuverability.

tion[3]. However, neither the tactical planners discussed above nor the trajectory planners are able to distinguish topologically distinct maneuver patterns. This can lead to "competing" locally optimal trajectories that belong to different patterns, which can further cause unstable behavior, e.g, cycle-to-cycle planning outcome oscillation (Fig. 2).

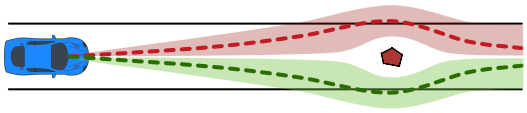

Fig. 2: The ignorance of topology in planning. The plot shows a pure path planning problem with a single static obstacle. Two homological/homotopic classes of paths exist: left (red region) and right (green region). There is a local optimal path within each class (the red/green dashed curves). Under symmetric cost definition, the two locally optimal paths can be very close (even tied) in cost, which causes indecisive alternation between the two locally optimal paths, which can further cause undesirable driving behaviors.

Topological trajectory planning algorithms have been studied in robotics. Triangulation [13], cell-decomposition [14], visibility-graph [14] and reference frame methods [15] have been developed to capture the topological structures of the robot's configuration space. Kuderer [16] and Park [17] proposed to perform topological analysis for mobile robots with Voronoi diagrams and cell decomposition respectively. However, these methods are limited to *co-terminal*[4] 2-D paths. Moreover, the need to generate the complete topology graph causes exponential growth in its size along with the number of obstacles. Finally, these methods are only easily applied in near-/relative-static environment. For example, Park [17] performed an experiment for freeway autonomous driving. However, a static snapshot of the moving obstacles is used to perform cell decomposition rather than taking into account the predicted motion of surrounding vehicles.

Inspired by electromagnetic theory, Bhattacharya [18] proposed to calculate an invariant "signature" to identify different homological 3-D paths. He further augmented the topological information to graph search to explore different homological paths. However, this method is also limited to co-terminal paths, which is not directly applicable to fixed-time-horizon spatiotemporal trajectory planning[5].

In this paper, we introduce the idea of fusing the traditional sampling-based trajectory planner with topological analysis to automatically discover and reason about tactical maneuver patterns, and guarantee the feasibility of the trajectory plan. We propose pseudo-homology to classify topologically different trajectories that are not necessarily co-terminal. This planner is evaluated in several on-road driving scenarios with time-varying surrounding objects for obstacle avoidance, lane-change and intersection handling.

[3]Often calculated as a scalar value defined as the weighted sum of multiple cost (feature) terms

[4]Co-terminal paths have the same starting point and destination point.

[5]The terminal states up to the sampled time horizon do not converge into a single space-time state, i.e., the trajectories are not co-terminal.

III. Theoretical Background

In topological trajectory planning, the distinction between path homology[6] and homotopy[7] must be clarified. In Fig. 3, $\mathcal{T}'$ and $\mathcal{T}''$ are homological: the loop formed by $\mathcal{T}'$ and $\mathcal{T}''$ does not contain any obstacle ring[8]. However, $\mathcal{T}'$ and $\mathcal{T}''$ are not homotopic, since they cannot be deformed from one to the other when two obstacle rings exist at the same time. In general, lemma 3.1 holds:

Lemma 3.1: Homotopy is a sufficient but unnecessary condition of homology.

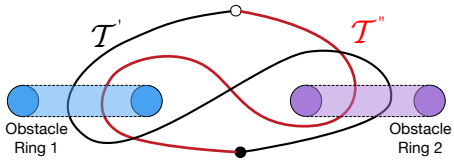

Fig. 3: Two homological 3-D paths $\mathcal{T}'$ and $\mathcal{T}''$ navigate through two obstacle rings. However, they are not homotopic since it is impossible to deform one to the other without intersecting obstacles.

The electromagnetism laws are useful for calculating invariant quantity for homological 3-D paths:

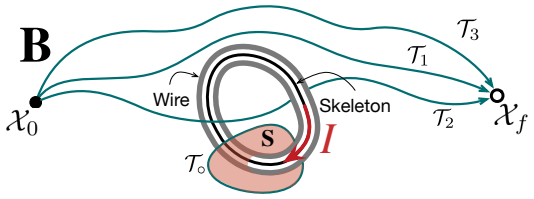

Fig. 4: Energized wire and its generated magnetic field in the 3-D Euclidean space. The current in the wire is I, and its enclosed surface is denoted by $\mathbf{S}$. Three co-terminal 3-D paths $\mathcal{T}_1$, $\mathcal{T}_2$ and $\mathcal{T}_3$ are further depicted starting at $\mathcal{X}_0$ and ending at $\mathcal{X}_f$. $\mathcal{T}_1$ and $\mathcal{T}_3$ are homological/homotopic since they both go around the (looped) wire $\mathcal{W}$, while $\mathcal{T}_2$ is not homological/homotopic to them .

Biot-Savart Law: a steady current flowing through a wire $\mathcal{W}$ generates the magnetic field $\mathbf{B}$, the vector value of which defined at $\mathcal{X} \in \mathbb{R}^3$ is:

$$\mathbf{B}(\mathcal{X}) = \frac{\mu_0 \cdot I}{4\pi} \int_{\mathcal{W}} \frac{\boldsymbol{l} - \mathcal{X}}{\|\boldsymbol{l} - \mathcal{X}\|^3} \cdot d\boldsymbol{l} \tag{1}$$

where I is the current in $\mathcal{W}$, $\boldsymbol{l}$ is a point on $\mathcal{W}$, and μ_0 is the magnetic constant, whose value is not significant for the purpose of homotopy analysis.

Ampere's Law: given a magnetic field $\mathbf{B}$ and a closed path $\mathcal{T}_\circ$, the line integral along $\mathcal{T}_\circ$ is proportional to the total current I passing through a surface $\mathbf{S}$ enclosed by $\mathcal{T}_\circ$

$$\oint_{\mathcal{T}_\circ} \boldsymbol{B} \cdot d\boldsymbol{l} = \mu_0 \cdot I \tag{2}$$

The laws of **Biot-Savart** and **Ampere** are dual theorems relating the energized looped wire $\mathcal{W}$ and the magnetic field

[6]Homological paths are co-terminal, and the boundary formed by connecting tail-to-head does not contain/collide with any obstacle.

[7]Homotopic paths are co-terminal, and deformable from one to the other without intersecting any obstacle.

[8]This can be tested by removing any single obstacle ring.

generated. In Fig. 4, regardless of the shape of the closed path $\mathcal{T}_\circ$, the integration of magnetic field $\boldsymbol{B}$ gives an *Ampere invariant* which is only relevant to the amount of current going through the closed surface $\mathbf{S}$ formed by $\mathcal{W}$.

In Bhattacharya [18], this property is exploited to define the $\mathcal{H}$ function for co-terminal paths like $\mathcal{T}_1$, $\mathcal{T}_2$, $\mathcal{T}_3$. Imagine planning with one (or more) ring-like obstacle, which is energized with current I and generates a magnetic field $\boldsymbol{B}$ like the wire $\mathcal{W}$ in Fig. 4. The $\mathcal{H}$ function is defined as the integration of the magnetic field $\boldsymbol{B}$ along $\mathcal{T}$:

$$\mathcal{H}(\mathcal{T}) = \int_{\mathcal{T}} \boldsymbol{B} \cdot d\boldsymbol{l}$$

It can also be shown that the $\mathcal{H}$ function gives a numerical equivalent to homology:

Theorem 3.2: paths $\mathcal{T}'$ and $\mathcal{T}''$ are homological if and only if their $\mathcal{H}$ functions are equal.

Note that whether the looped wire has volume is irrelevant to the result of topological analysis. The deformable retract[9] of an object $\mathcal{O}$ is its homology/homotopy equivalent, or its skeleton $\mathcal{S}(\mathcal{O})$. In Fig. 4, a 1-D curved skeleton $\mathcal{S}(\mathcal{W})$ is obtained by "shrinking" the wire $\mathcal{W}$. Replacing $\mathcal{W}$ with $\mathcal{S}(\mathcal{W})$ does not change the homology/homotopy relationship among $\mathcal{T}_1$, $\mathcal{T}_2$ or $\mathcal{T}_3$.

IV. Spatiotemporal Topological Analysis

The planning workspace of the autonomous vehicle considered in this paper is a 3-D spatiotemporal space $\mathbb{W} = [\mathbb{R}^2 \times \mathbb{T}]$ obtained by augmenting a 2-D planar space $\mathbb{R}^2$ with a time dimension $\mathbb{T}$. A bounded workspace $\overline{\mathbb{W}}$ is considered in practice due to fixed horizon (T) at every planning cycle.

Taking the surrounding objects[10] into account is the primary goal of motion planning for urban autonomous driving. Taking a snapshot at any given time, an object is represented as a 2-D polygon. Adding the temporal prediction (up to T) to a 2-D object creates a 3-D temporal object. Fig. 5a shows an on-road driving scenario with a single bicyclist as the object to avoid. The bicyclist object $\mathcal{O}$ is augmented as a pillar-shaped temporal object in $\mathcal{O}^{\overline{\mathbb{W}}}$ within $\overline{\mathbb{W}}$, with its predicted trajectory (Fig. 5b) as its skeleton $\mathcal{S}(\mathcal{O}^{\overline{\mathbb{W}}})$.

However, $\mathcal{O}^{\overline{\mathbb{W}}}$ is not able to incur different homological/homotopic trajectories because it is genus[11]-0. In order to introduce this ability, augmented temporal objects $\mathcal{O}^{\mathbb{W}}$ of genus-1 are created by augmenting $\mathcal{O}^{\overline{\mathbb{W}}}$ with a loop-like structure in the space $\mathbb{W}/\overline{\mathbb{W}}$ ($\{x | x \in \mathbb{W}, x \notin \overline{\mathbb{W}}\}$). This can be achieved by appending either a finite loop giving $\mathcal{O}^{\overline{\mathbb{W}}}_\circ$ (Fig. 5c) or through an infinity loop giving $\mathcal{O}^{\overline{\mathbb{W}}}_\infty$ (Fig. 5d). The latter, in a fashion that extends both ends of the skeleton to infinity in parallel to the time dimension, is preferred for its mathematical simplicity. The virtual magnetic field

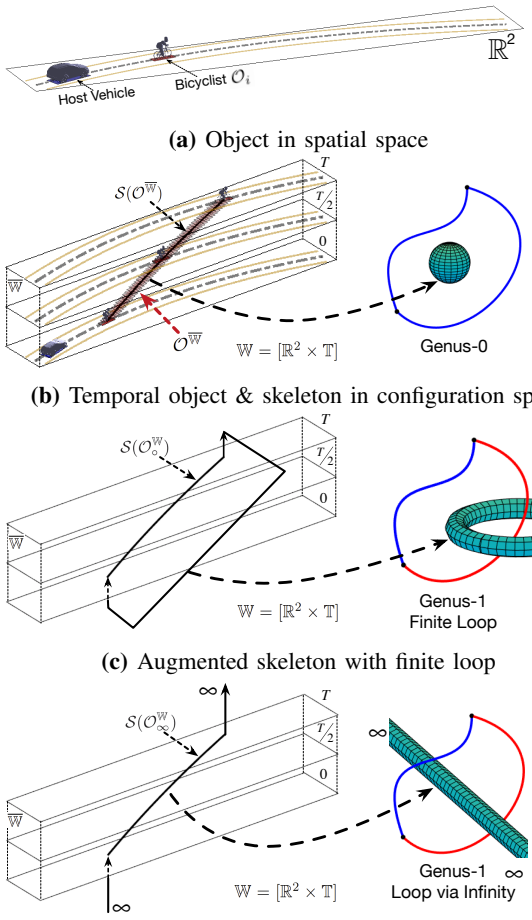

(a) Object in spatial space

(b) Temporal object & skeleton in configuration space

(c) Augmented skeleton with finite loop

(d) Augmented skeleton with loop through infinity

Fig. 5: The creation of a genus-0 temporal object, its genus-1 augmentation and the virtual magnetic field incurred in the configuration space. (a) shows the 2-D spatial space $\mathbb{R}^2$ with the host vehicle and a moving bicyclist $\mathcal{O}$. (b) shows the 3-D spatiotemporal workspace $\mathbb{W}$ and its bounded subspace $\overline{\mathbb{W}}$. It also shows the temporal object $\mathcal{O}^{\overline{\mathbb{W}}}$ created from the moving bicyclist $\mathcal{O}$, and its skeleton $\mathcal{S}(\mathcal{O}^{\overline{\mathbb{W}}})$. (c) shows the skeleton of an augmented temporal object $\mathcal{S}(\mathcal{O}^{\mathbb{W}}_\circ)$ from outside of the bounded workspace. (d) shows the skeleton of an augmented temporal object $\mathcal{S}(\mathcal{O}^{\mathbb{W}}_\infty)$ through infinity.

is further obtained via integration along $\mathcal{S}(\mathcal{O}^{\overline{\mathbb{W}}}_\infty)$ to calculate the $\mathcal{H}$ function discussed in section III. A trajectory in $\mathbb{W}$ is equivalent to a path in $\mathbb{R}^3$. The property of the $\mathcal{H}$ function holds for $\mathbb{W}$.

Furthermore, instead of only analyzing co-terminal paths, it is of practical interest to group trajectories that terminate in the same 2-D spatial region $\mathbb{R}^2$ for on-road driving. Pseudo-homology is therefore formally defined:

Pseudo-homology: two paths $\mathcal{T}'$ and $\mathcal{T}''$ are pseudo-homological if they both start from the same state and end in the same path-connected region $\mathcal{R} \in \mathbb{R}^2$.

Similar to the 1-D skeleton being the deformable retract of a 3-D object, a 0-D point is the retract of a 2-D spatial region $\mathcal{R}$. This point is also referred to as the representative point $\mathcal{X}^*_\mathcal{R}$ of $\mathcal{R}$. Note that $\mathcal{R}$ does not have to be a convex shape, and the exact location of $\mathcal{X}^*_\mathcal{R}$ is insignificant as long

[9]Deformable retract is a continuous mapping from the entire space (object) into a subspace (skeleton) completely contained within. The subspace does not alter the topology exhibited by the surface of the original space.

[10]E.g., static objects, surrounding traffic, bicyclist, pedestrian, etc.

[11]Genus is an important concept in algebraic topology [19]. An intuitive interpretation of genus is the maximum number of "cuts" that can be performed on an object such that the cut object is still a connected object with full volume, e.g., in 3-D, a ball is genus-0, a loop hole is genus-1, etc.

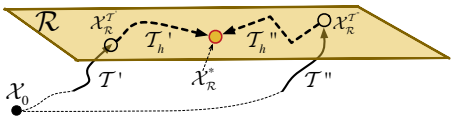

Fig. 6: Pseudo-homological trajectories. Trajectories $\mathcal{T}'$ and $\mathcal{T}''$ are pseudo-homological since they both start from state $\mathcal{X}_0$, and end in the same path-connected region $\mathcal{R} \in \mathbb{R}^2$ at states $\mathcal{X}_{\mathcal{R}}^{\mathcal{T}'}$ and $\mathcal{X}_{\mathcal{R}}^{\mathcal{T}''}$. A representative state $\mathcal{X}_{\mathcal{R}}^*$ is specified for $\mathcal{R}$, and helper trajectories $\mathcal{T}_h'$, $\mathcal{T}_h''$ in $\mathcal{R}$ connect the original trajectories to $\mathcal{X}_{\mathcal{R}}^*$.

as it is contained by $\mathcal{R}$. Then the following corollary is used to efficiently test for pseudo-homology:

Corollary: two trajectories $\mathcal{T}'$ and $\mathcal{T}''$ are pseudo-homological if they can be extended from where they terminate on $\mathcal{R}$ to $\mathcal{X}_{\mathcal{R}}^*$ with helper trajectories $\mathcal{T}_h'$ and $\mathcal{T}_h''$, and

$$\mathcal{H}(\mathcal{T}' + \mathcal{T}_h') = \mathcal{H}(\mathcal{T}'' + \mathcal{T}_h'')$$

The helper trajectories can be of arbitrary shape, as long as they stay within $\mathcal{R}$ (Fig. 6). The procedure to determine the pseudo-homology is summarized by algorithm 1:

Algorithm 1 Determine pseudo-homology

Require: Two trajectories $\mathcal{T}'$ and $\mathcal{T}''$
Ensure: Correct judgment of trajectories' pseudo-homology
  IDENTIFY a spatial region $\mathcal{R} \in \mathbb{R}^2$ within $\overline{\mathbb{W}}$ at time T.
  CHECK if the end states $\mathcal{X}^{\mathcal{T}'}$ and $\mathcal{X}^{\mathcal{T}''}$ are in $\mathcal{R}$.
    IF no, **RETURN** false
  RETRACT region $\mathcal{R}$ to a representative point $\mathcal{X}_{\mathcal{R}}^*$
  CONSTRUCT helper trajectories $\mathcal{T}_h'$ and $\mathcal{T}_h''$ that connect $\mathcal{X}_{\mathcal{R}}^{\mathcal{T}'}$ and $\mathcal{X}_{\mathcal{R}}^{\mathcal{T}''}$ to $\mathcal{X}_{\mathcal{R}}^*$
  CALCULATE the $\mathcal{H}$ function of $\mathcal{T}' + \mathcal{T}_h'$ and $\mathcal{T}'' + \mathcal{T}_h''$
    IF $\mathcal{H}(\mathcal{T}' + \mathcal{T}_h') \neq \mathcal{H}(\mathcal{T}'' + \mathcal{T}_h'')$ **RETURN** false
    ELSE RETURN true

Algorithm 1 plays a key role in behavioral discovery in section V for its efficient topological distinguishing capability as well as its region-awareness.

V. Fused Tactical Maneuver Discovery, Reasoning & Motion Planning

The fusion of tactical maneuver discovery/reasoning and trajectory planning is achieved in three steps. A pool of feasible and admissible trajectory candidates is first sampled. From this pool, distinct tactical maneuver patterns are automatically extracted along with their semantic interpretation. Then the final trajectory is obtained by first deciding on a tactical pattern, followed by choosing the optimal trajectory belonging to the selected pattern.

A. Trajectory sampling

Trajectory samples must first be generated to form a pool of possible maneuver candidates, the foundation of which is the motion primitives that connect one state to another in a smooth fashion. Decoupled/analytical primitives [20], [21] are used. They allow the trajectory evaluation routine to be broken into steps, checking for path collision against static objects first before checking for the trajectory, which can save computation time by eliminating infeasible spatiotemporal trajectory search nodes at an early stage. Their analytical solution allows for trivial computation overhead rather than an iterative optimization effort.

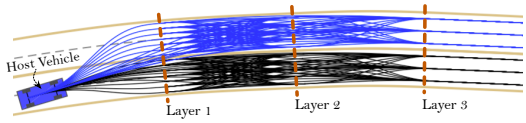

Fig. 7: Path sampling pattern for on-road driving. The black curves represent the path candidates sampled in the current lane of the host vehicle, while the blue curves represent those in the neighboring lane. Each group of paths is sampled by placing three layers of terminal states along the road with decreasing lateral alternatives.

Another important choice is the sampling pattern, which determines the subspace of the spatiotemporal domain that the planner should focus on exploring. There is a trade-off between sampling exhaustiveness and the computation overhead. We adopt the classical patterns for on-road driving [8], [9], which involve sampling paths along the road (Fig. 7) and expanding the spatiotemporal search space by branching over the sampled polynomial speed profiles. All the trajectories are sampled up to a fixed lookahead time horizon T (the next few seconds) to represent a short-term maneuver.

B. Maneuver-based tactics discovery

Given the trajectory pool, the next goal is to discover the maneuver-based tactical patterns and their semantic descriptions. Different patterns can be extracted depending on the spatial area where the trajectory terminates (**region-based distinction**), how it gets there around the obstacles (**homology-based distinction**), and what overtaking (if any) order it follows (**sequence-based distinction**).

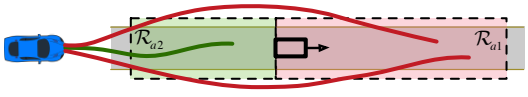

(a) Region-based distinction for in-lane object.

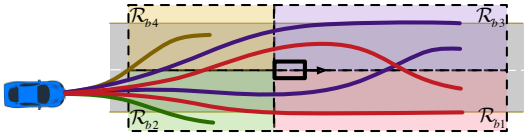

(b) Region-based distinction for inter-lane object.

Fig. 8: Region-based and homology-based distinctions for on-road driving. (a) shows two corridor regions can be distinguished, $\mathcal{R}_{a1}$ and $\mathcal{R}_{a2}$, for an object in a one-lane road. (b) shows four regions are distinguished, $\mathcal{R}_{b1}$, $\mathcal{R}_{b2}$, $\mathcal{R}_{b3}$ and $\mathcal{R}_{b4}$, for an object on a two-lane road. For each region $\mathcal{R}$, there are one or two curves in darker color representing the possible homological trajectories whose terminal states are in $\mathcal{R}$.

Region-based Distinction: an object on a single-lane road naturally splits the lane into front/back corridor-like regions (Fig. 8a). Region-based pattern distinction is defined by which region a trajectory terminates in: object overtaking ($\mathcal{R}_{a1}$) or following ($\mathcal{R}_{a2}$). For an object on a two-lane

road (Fig. 8b), four regions can be distinguished: right-lane overtaking ($\mathcal{R}_{b1}$), right-lane following ($\mathcal{R}_{b2}$), left-lane overtaking ($\mathcal{R}_{b3}$) and left-lane following ($\mathcal{R}_{b4}$).

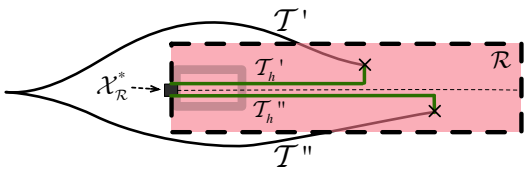

Fig. 9: Retracted point for an on-road region and the construction of helper trajectories for maneuver pattern extraction. The red region is a goal region $\mathcal{R} \in \mathbb{R}^2|_T$ implied by an object. The black rectangle is the retracted representative point $\mathcal{X}_{\mathcal{R}}^*$ of $\mathcal{R}$. The two black curves are the sampled trajectories $\mathcal{T}', \mathcal{T}''$ that start from the same position and both end in $\mathcal{R}$. The green curves are the two helper trajectories $\mathcal{T}_h', \mathcal{T}_h''$ that connect the original trajectories to $\mathcal{X}_{\mathcal{R}}^*$.

Homology-based Distinction: trajectories may reach the same tactical region by taking topologically different paths, which is another important aspect of maneuver-based tactics. For each region in Fig. 8, all the topologically distinctive trajectories are depicted in the same color. Algorithm 1, which determines trajectory pseudo-homology, has been used for the homology-based distinction.

Efficient ways to determine the representative point and construct helper trajectories for each identified region are required by the algorithm. Taking advantage of the fact that the region $\mathcal{R}$ (Fig. 9) is constructed from corridor-like on-road lanes, we place $\mathcal{X}_{\mathcal{R}}^*$ on the centerline, close to the region boundary near the object itself. The helper trajectories are then constructed by connecting from the location where the trajectory terminates in the region, to the projected point perpendicular to the centerline, and further moving along the centerline to reach $\mathcal{X}_{\mathcal{R}}^*$.

Sequence-based Distinction: in fact, only "overtaking" regions may introduce different homological plans. When "overtaking" behaviors for multiple objects are considered, it is important to know not just topological information, but also the temporal sequence of overtaking behavior, which is used as an additional cue to distinguish different maneuver patterns.

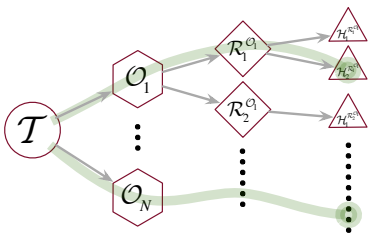

Fig. 10: Distinction tree generated for N-object.

Suppose N objects are actively considered for patterns. Each object can incur multiple region-based distinctions, which further incur additional homology-based distinctions. A distinction tree (Fig. 10) lists distinguishable maneuver patterns for each object considered. A maneuver-based tactical pattern can be defined as a unique sequence of N routes in the distinction tree from the root to the leaf nodes:

$$\mathcal{L} = \begin{bmatrix} \mathcal{L}_1 \\ \vdots \\ \mathcal{L}_N \end{bmatrix} = \begin{bmatrix} \mathcal{T} \to \mathcal{O}_1 \to \mathcal{R}_i^{\mathcal{O}_1} \to \mathcal{H}_j^{\mathcal{R}_i^{\mathcal{O}_1}} \\ \vdots \\ \mathcal{T} \to \mathcal{O}_N \to \mathcal{R}_i^{\mathcal{O}_N} \to \mathcal{H}_j^{\mathcal{R}_i^{\mathcal{O}_N}} \end{bmatrix}$$

where N is the number of objects in consideration, $i = 1, \ldots, A$, A is the number of region-based distinctions for each object $\mathcal{O}$, $j = 1, \ldots, B$, and B is the number of homology-based distinctions for each $\mathcal{R}_i^{\mathcal{O}}$. Each entry is represented by a green route in Fig. 10.

With patterns identified, trajectories can be grouped together accordingly, which concludes the tactical maneuver pattern discovery process. Note that while the number of possible patterns grows exponentially as the number of objects increases[12], the runtime of our planner is bounded by the number of trajectories. Also, the computation needed for evaluating the $\mathcal{H}$ function on each trajectory grows linearly, rather than exponentially.

C. Fused decision making & trajectory planning

Two subsequent steps naturally arise: choosing the pattern and the final trajectory. The choices of both depend on quantitative evaluation with cost functions. The cost function is defined as a weighted accumulation of multiple trajectory-based feature terms. Commonly used features are the closest distance to an object, the average/maximum speed, the average/maximum longitudinal/lateral acceleration, and the average/maximum deviation from the lane centerline [2], [8], [9], [22].

New features are proposed to quantify penalties for tactical patterns. First, some generative features can be extracted by averaging the trajectory-based features within a particular tactical maneuver pattern. Moreover, an efficiency feature cost that favors the pattern with greater longitudinal traversal along the lane is designed, since it resembles greater on-road driving progress made within a fixed horizon. In addition, a consistency feature is calculated to measure the degree of pattern change from the last planning cycle:

$$\sum_{i=1}^{M} \delta(\mathcal{L}_i \neq \mathcal{L}_i')$$

where M is the number of common objects that exist both in the current and last planning cycle, $\mathcal{L}_i$ and $\mathcal{L}_i'$ are the routes of the i^{th} common object in the current and last distinction trees respectively, and

$$\delta(\mathcal{A}) = \begin{cases} 1, & \text{if statement } \mathcal{A} \text{ is } \textit{TRUE} \\ 0, & \text{if statement } \mathcal{A} \text{ is } \textit{FALSE} \end{cases}$$

which makes it less likely to switch among different patterns between planning cycles, unless absolutely necessary.

[12]One in-lane object introduces 3 maneuver patterns, two introduce 9, three introduce 27, etc...

VI. Results

The proposed maneuver discovery methods are applied in three urban driving scenarios:

- $\mathcal{S}_1$: one bicyclist and one static object in a single-lane situation (Fig. 11).
- $\mathcal{S}_2$: the host vehicle needs to perform a lane-change when there is also a slow-moving bicyclist in the middle of the current lane (Fig. 12).
- $\mathcal{S}_3$: one pedestrian crossing in front of the host vehicle at a T-intersection and two moving cars in the target lane (Fig. 13).

For each scenario, feasible maneuver patterns are first obtained with the optimal trajectories of each pattern:

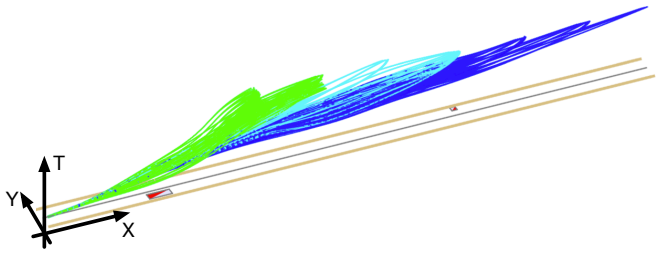

(a) Spatiotemporal trajectory samples.

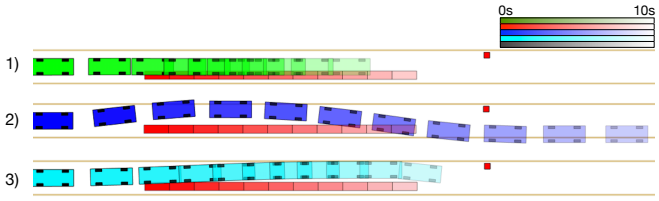

(b) Discovered tactical patterns and optimal trajectories.

Fig. 11: Scenario 1: avoid a bicyclist and a static object in a single lane. (a) shows the spatiotemporal trajectory samples. Three tactical maneuver patterns are identified, and trajectories of the same pattern are grouped together in the same color. (b) shows the optimal trajectory of each maneuver pattern, along with the predicted motion of surrounding objects.

For scenario $\mathcal{S}_1$, three patterns are identified (Fig. 11a), and the optimal trajectories of each pattern are further obtained (Fig. 11b).

1) the host vehicle slows down to follow the bicyclist. Both objects will be avoided in a conservative fashion, i.e., no overtaking.
2) the host vehicle mildly slows down to overtake the bicyclist, and performs a double swerve to avoid both objects.
3) the host vehicle overtakes the bicyclist, and stops in front of the static obstacle.

For scenario $\mathcal{S}_2$, three patterns are identified, represented by the optimal trajectory of each pattern:

1) the host vehicle slows down to stay behind the bicyclist. Lane-change is halted indefinitely.
2) the host vehicle slows down to merge into the target lane after both cars in the target lane pass by.
3) the host vehicle slightly accelerates to merge into the gap between the two cars in the target lane.

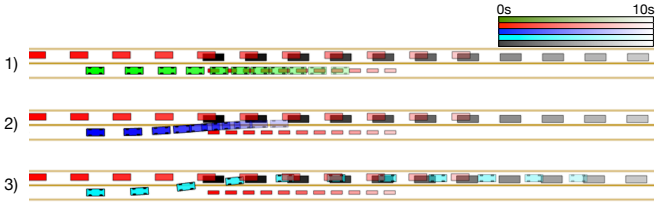

Fig. 12: Scenario 2: lane change in traffic with an obstacle in the middle of the current lane.

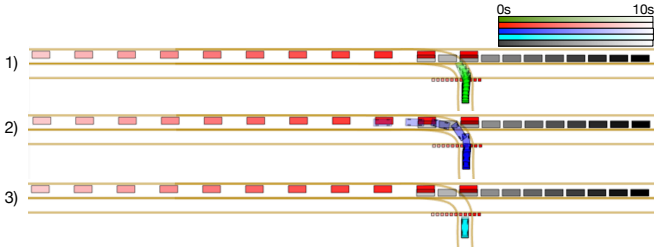

Fig. 13: Scenario 3: enter traffic from stationary start at T-intersection with pedestrian and traffic. The figure shows the discovered patterns, the optimal trajectory for each pattern, and the predicted motion of surrounding objects.

For scenario $\mathcal{S}_3$, three patterns are identified, represented by the optimal trajectory of each pattern:

1) the host vehicle moves after the pedestrian crosses the road, and merges to follow the second car.
2) the host vehicle accelerates before the pedestrian crosses the road to merge into the gap between the first and the second car.
3) the host vehicle stays behind the pedestrian, halting merging indefinitely.

The maneuver pattern is further selected based on pattern-level reasoning, which is dependent on the weightings on the progress/aggressiveness/consistency features. The optimal trajectory within the selected pattern is then found for the final planning output.

To highlight the benefit of distinguishing tactical maneuver patterns in the traditional optimal planning method, we implement a pure cost function-based motion planner whose sampling pattern and trajectory-level cost function are identical to the proposed planner. They are tested side-by-side in scenario $\mathcal{S}_4$ (Fig. 14), which consists of a single static object in the center of the lane with some sensing noise added.

In Fig. 14a, the sensor uncertainty tends to cause indecisive (alternating) planning outcomes from the pure cost function-based planner. The proposed planner, on the other hand, sticks to swerving around the static object from one side (Fig. 14b), which demonstrates superior plan consistency. The difference results from the explicit exposure of maneuver patterns, and the consideration of the "consistency" feature in the pattern-level reasoning.

VII. Conclusion

In this paper, we propose an automated maneuver-based tactical pattern discovery/reasoning methodology fused with

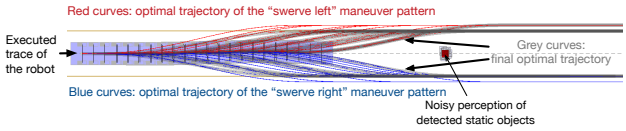

(a) Performance by the pure cost function-based planner.

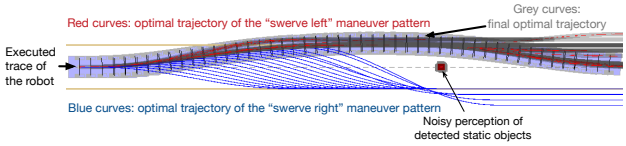

(b) Performance by the proposed fused planer.

Fig. 14: Scenario 4: improved planning coherency. (a) demonstrates the performance of the baseline pure cost function-based planner, which yields an indecisive cycle-by-cycle planning outcome. (b) shows the performance of the proposed fused planner, which demonstrates a consistent planning outcome.

sampling-based trajectory planning for on-road autonomous driving. The concept of pseudo-homology is introduced by relaxing the co-terminal requirements on trajectories. The pattern discovery routine is achieved by clustering groups of trajectories with unique region-/homology-/sequence-based distinctions. Finally, cost function-based pattern-level and trajectory-level reasoning are used to determine the final pattern/trajectory in execution.

In summary, the three challenges raised in Section I are adequately addressed. A specific maneuver-based tactical pattern is decided upon only after all the feasible and admissible trajectories are constructed and evaluated, which addresses **challenge 1**. Second, the method enables the planner to be explicitly aware of the environment's topology structure and behave similarly to how an experienced human driver sticks to a route, which addresses **challenge 2**. Finally, regardless of how the environment changes, the proposed method demonstrates the ability to automatically identify different tactical maneuver patterns to reason about, which addresses **challenge 3**.

This work motivates the idea of using pseudo-homology along with characterizing workspace regions as a formal theoretical tool in extracting/semanticizing high-level tactical maneuver patterns, which can be extended to many other motion planning applications, such as manipulators and unmanned aerial vehicles. In future work, the proposed algorithm will be extended to distinguish subtle maneuver patterns with more complex reasoning capability.

REFERENCES

[1] M. Buehler, K. Iagnemma, and S. Singh, *The DARPA urban challenge: autonomous vehicles in city traffic*. 2009.

[2] C. Urmson *et al.*, "Autonomous driving in Urban environments: Boss and the Urban Challenge," *Springer Tracts in Advanced Robotics*, vol. 56, pp. 1–59, aug 2009.

[3] A. Bacha *et al.*, "Odin: Team victorTango's entry in the DARPA urban challenge," *Journal of field Robotics*, vol. 25, no. 8, pp. 467–492, 2008.

[4] S. Kammel *et al.*, "Team AnnieWAY s Autonomous System for the 2007 DARPA Urban Challenge," in *Journal of Field Robotics*, vol. 25, pp. 615–639, Springer, 2008.

[5] J. Hurdus *et al.*, "VictorTango Architecture for Autonomous Navigation in the DARPA Urban Challenge," in *Journal of Aerospace Computing, Information, and Communication*, vol. 5, pp. 506–529, Springer London, 2008.

[6] P. Pirjanian, "Behavior Coordination Mechanisms-state-of-the-art," *Ethology*, vol. 1, no. 213, pp. 1–49, 1999.

[7] M. Pivtoraiko *et al.*, "Differentially constrained mobile robot motion planning in state lattices," *Journal of Field Robotics*, vol. 26, no. 3, pp. 308–333, 2009.

[8] J. Ziegler and C. Stiller, "Spatiotemporal state lattices for fast trajectory planning in dynamic on-road driving scenarios," in *2009 IEEE/RSJ International Conference on Intelligent Robots and Systems, IROS 2009*, pp. 1879–1884, IEEE, 2009.

[9] M. Mcnaughton and C. Urmson, *Parallel Algorithms for Real-time Motion Planning*. PhD thesis, 2011.

[10] W. Xu, J. Wei, J. M. Dolan, H. Zhao, and H. Zha, "A Real-Time Motion Planner with Trajectory Optimization for Autonomous Vehicles," in *Robotics and Automation (ICRA), 2012 IEEE International Conference on*, pp. 2061–2067, IEEE, 2012.

[11] J. Ziegler, P. Bender, T. Dang, and C. Stiller, "Trajectory planning for Bertha - A local, continuous method," in *IEEE Intelligent Vehicles Symposium, Proceedings*, pp. 450–457, 2014.

[12] S. Wang, *State Lattice-based Motion Planning for Autonomous On-Road Driving*. PhD thesis, 2015.

[13] D. Demyen and M. Buro, "Efficient triangulation-based pathfinding," *Aaai*, 2006.

[14] H. M. Choset, *Principles of robot motion: theory, algorithms, and implementation*. MIT press, 2005.

[15] K. D. Jenkins, "The Shortest Path Problem in the Plane with Obstacles: A Graph Modeling Approach to Producing Finite Search Lists of Homotopy Classes," jun 1991.

[16] M. Kuderer and C. Sprunk, "Online generation of homotopically distinct navigation paths," ... *and Automation (ICRA* ..., 2014.

[17] J. Park, "Homotopy-Based Divide-and-Conquer Strategy for Optimal Trajectory Planning via Mixed-Integer Programming," ... , *IEEE Transactions on*, 2015.

[18] S. Bhattacharya, M. Likhachev, and V. Kumar, "Topological constraints in search-based robot path planning," *Autonomous Robots*, vol. 33, no. 3, pp. 273–290, 2012.

[19] A. Hatcher, "Algebraic topology. 2002," *Cambridge UP, Cambridge*.

[20] A. Piazzi and C. G. L. Bianco, "Quintic G 2-splines for trajectory planning of autonomous vehicles," in *Intelligent Vehicles Symposium, 2000. IV 2000. Proceedings of the IEEE*, pp. 198–203, IEEE, 2000.

[21] J. W. Lee and B. Litkouhi, "A unified framework of the automated lane centering/changing control for motion smoothness adaptation," in *IEEE Conference on Intelligent Transportation Systems, Proceedings, ITSC*, pp. 282–287, IEEE, 2012.

[22] T. Gu, J. Snider, J. M. Dolan, and J. W. Lee, "Focused Trajectory Planning for autonomous on-road driving," in *IEEE Intelligent Vehicles Symposium, Proceedings*, no. Iv, pp. 547–552, IEEE, 2013.